

## ARTICLE OPEN



# Possible impacts of vegetation cover increment on the relationship between winter snow cover anomalies over the Third Pole and summer precipitation in East Asia

Kai Yang<sup>1</sup>✉, Qi Qi<sup>1</sup> and Chenghai Wang<sup>1</sup>✉

Snow cover over the Tibetan Plateau (TP)—the Third Pole of the earth has been recognized as a reliable signal of summer floods or droughts in East Asia (EA). The distribution of snow cover can be influenced by vegetation, however, the impacts of changes in cover of non-growing season vegetation—withered grass stem over TP on the climatic effects of snow cover remains poorly understood. Here, we showed that the relationship between TP winter snow cover (TPWSC) and EA summer precipitation (EASP) strengthened starting in the early 1990s but weakened after the early 2000s. The weakening of the TPWSC–EASP relationship was linked to the effects of vegetation cover increment (VCI) on winter and spring snow cover over the TP. A possible mechanism behind this linkage is that VCI leads to a shortened persistence of TPWSC anomalies and weakened surface diabatic heating anomalies in spring. Consequently, the influences of TP thermal forcing on the downstream atmospheric circulation in summer were altered, resulting in a different pattern of EASP anomalies. These findings highlight the importance of snow–vegetation feedback and its potential to alter the effectiveness of snow cover in seasonal climate prediction.

*npj Climate and Atmospheric Science* (2023)6:140; <https://doi.org/10.1038/s41612-023-00467-3>

## INTRODUCTION

Snow cover plays a crucial role in the Earth system through its high albedo and hydrological effects<sup>1–7</sup>. The climatic effects of snow cover anomalies at high-latitude and high-altitude regions have long been acknowledged. The earliest study<sup>8</sup> demonstrated a significant relationship between snow cover in the Himalayas and the Indian summer monsoon. After that, studies further revealed that winter–spring snow cover over the TP has a notable connection with summer atmospheric circulation and precipitation in East Asia (EA)<sup>9–14</sup>. This relationship between snow cover and subsequent precipitation has been widely employed in seasonal climate prediction<sup>15,16</sup>.

Over the past few decades, snow cover over the TP has exhibited clear interannual and interdecadal variations<sup>10,17–19</sup>. Spring snowmelt, an essential aspect of snow cover anomalies influencing surface energy budget and soil water storage, is closely related to the snow cover in the preceding winter and springtime temperature<sup>20</sup>. In a warmer climate, along with the temperature increase, snowmelt in mountainous regions would slow down due to a shorter snowmelt season and reduced snow water equivalent<sup>21,22</sup>. As a result, the impacts of snow cover anomalies on subsequent climate are expected to undergo transitions. Recent studies have indicated that the relationship between spring snow cover and Indian summer monsoon rainfall has weakened since 1990 due to reduced lagged snow-hydrological effects<sup>23</sup>. Additionally, the relationship between TP snow cover anomalies and the subsequent climate in EA is non-stationary<sup>24,25</sup>, influenced by changes in the atmospheric circulation anomaly patterns and tropical sea surface temperature anomaly teleconnection. However, the inner mechanisms, such as the complex water–heat exchanges in snow–atmosphere coupling, linked to the changes in the relationship between snow cover anomalies and subsequent weather and climate remain elusive.

In addition to the terrain<sup>26</sup>, black carbon, and aerosols in snow<sup>27</sup>, short vegetation (e.g., grass) can also influence the snow cover through canopy radiative transfer<sup>28,29</sup>. Due to the shallow snow depth in most regions of the TP<sup>30</sup>, withered grass stems are generally not fully buried by snow, resulting in a lower surface albedo compared to the snow surface<sup>29</sup>. Consequently, the snow easily melts or sublimates with an increase in incident radiation. Notably, the vegetation over the TP has experienced significant growth in recent decades<sup>31</sup>, and the unburying of withered grass stems should influence snow cover during winter and spring. Hence, it is essential to further explore how changes in the cover of non-growing season vegetation—withered grass stems influence the lagged effects of snow cover.

This study focuses on two questions: how does the relationship between TP winter snow cover (TPWSC) and EA summer precipitation (EASP) change on an interdecadal scale? What is the linkage between the non-growing season vegetation cover increment (VCI) and changes in the TPWSC–EASP relationship? To address these questions, we examined the TPWSC–EASP relationship, explored the connection between changes in TP snow cover and VCI, and investigated possible physical mechanisms using long-term snow cover and depth data, gauge-based precipitation data, reanalysis datasets, and model simulations.

## RESULTS

### Interdecadal changes in the TPWSC–EASP relationship

We found that the interannual variability in TPWSC primarily occurs over the central-eastern TP, as evident from the leading EOF mode (EOF1) pattern for the winter snow cover fraction over the TP (Fig. 1a). Thus, we calculated the averaged winter snow cover fraction over central-eastern TP as an index of TPWSC that effectively represents its temporal variations (Supplementary Fig.

<sup>1</sup>Key Laboratory of Climate Resource Development and Disaster Prevention of Gansu Province, Research and Development Center of Earth System Model, College of Atmospheric Sciences, Lanzhou University, Lanzhou 730000, China. ✉email: yangkai@lzu.edu.cn; wch@lzu.edu.cn

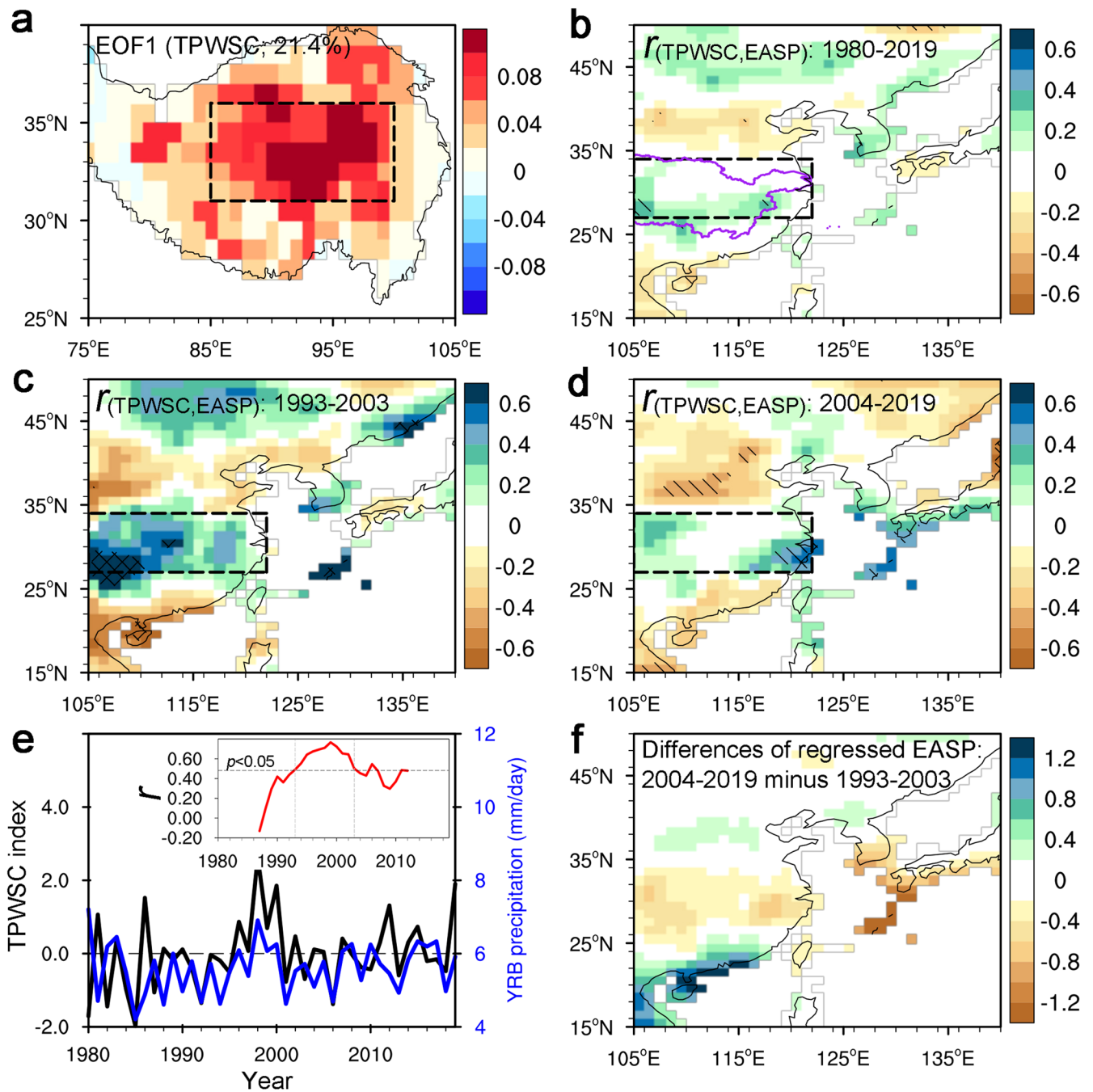


**Fig. 1** Changes in relationship between Tibetan Plateau (TP) winter snow cover (TPWSC) and East Asia (EA) summer precipitation (EASP). **a** Eigenvectors of the leading EOF mode (EOF1) for winter snow cover fraction over the TP. **b** Distributions of correlation coefficients ( $r$ ) of the EASP with the TPWSC index (see Methods) during 1980–2019; hatching and crosshatching shading represent the values significant at the  $p < 0.1$  and  $p < 0.05$  confidence levels based on Student's  $t$  test. **c**, **d** Same as **b** but for the correlations during 1993–2003 and 2004–2019. **e** Evolution of the TPWSC and summer precipitation averaged over the Yangtze River Basin (YRB; dashed rectangle in Fig. 1b), the inset line chart denotes a 15-year sliding correlation between TPWSC and EASP. **f** Difference of regressed EASP ( $\text{mm day}^{-1}$ ) by TPWSC index between 2004–2019 and 1993–2003. All datasets were detrended before the statistical analyses.

1; see Methods). The relationship between TPWSC and EASP was examined after removing the impacts of the ocean and other interdecadal and multidecadal oscillations (see Methods). The statistical analysis shows that TPWSC and EASP exhibit a positive correlation over the Yangtze River Basin (YRB), Indochina and Northeast China, while a negative correlation appears over South China, North China, and West Japan (Fig. 1b). However, the correlations between TPWSC and EASP during the 1980–2019 period passing the significance test ( $p < 0.1$  level) are weak.

We further examined the stability of the TPWSC–EASP relationship. For this analysis, the summer precipitation averaged over YRB was calculated as the representation of EASP. As shown in Fig. 1e, both TPWSC and YRB summer precipitation exhibit prominent interannual variability (both time series were detrended; see Methods). The 15-year sliding correlations between TPWSC and YRB summer precipitation experienced significant shifts on an interdecadal scale (see inset in Fig. 1e). Around the early 1990s, there was a strengthening relationship between the TPWSC and

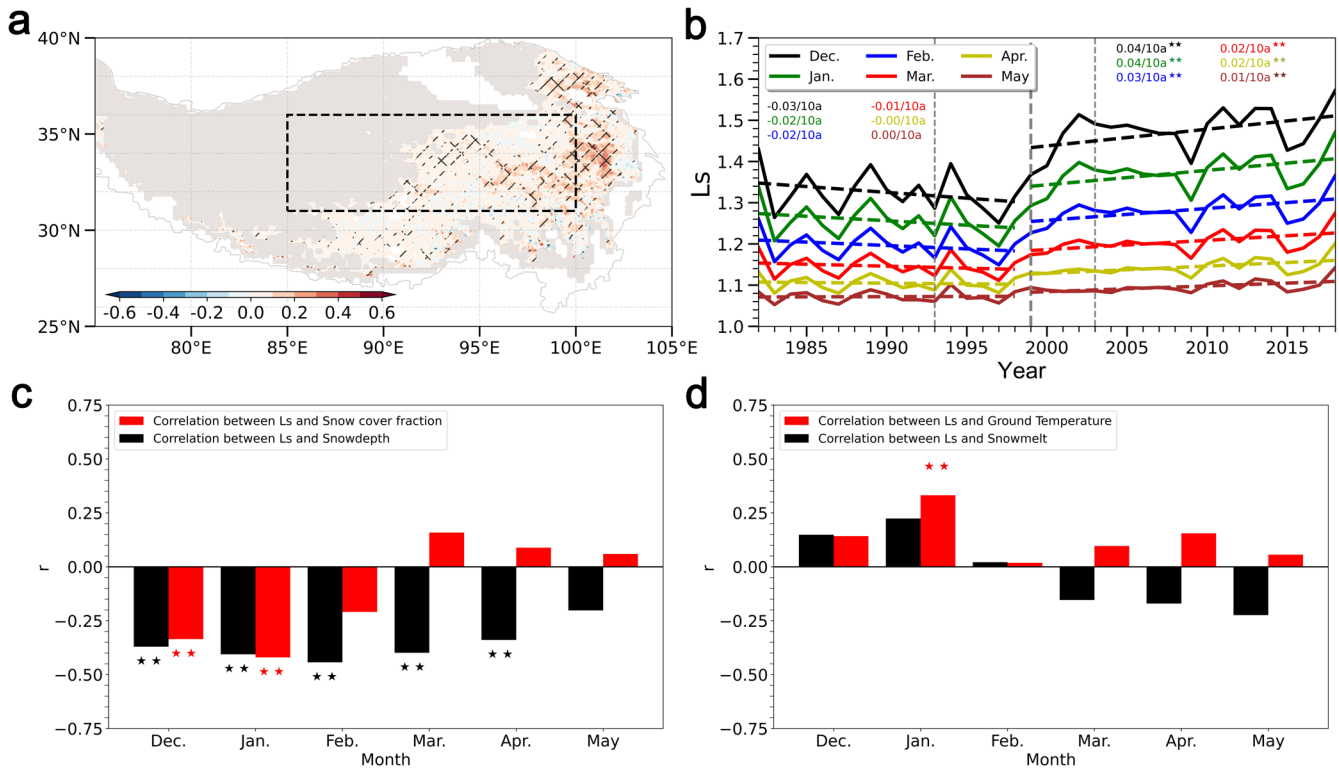


**Fig. 2** Variations of withered grass stem area and its linkage with the snow cover and ground temperature in winter and spring over TP. **a** Distribution of linear trend coefficients ( $\text{decade}^{-1}$ ) of withered grass stem area index ( $L_s$ ; see in Methods) during 1982–2018, hatching and crosshatching shading represent the values significant at the  $p < 0.1$  and  $p < 0.05$  confidence levels based on Student's  $t$  test, the grey shading represents the underlying surface outside of the grassland. **b** Evolutions of  $L_s$  averaged over the central-eastern TP ( $31^\circ\text{--}36^\circ\text{N}$ ,  $85^\circ\text{--}100^\circ\text{E}$ ; dashed rectangle in Fig. 2a). **c** Correlations ( $r$ ) of  $L_s$  with snow depth and snow cover fraction. **d** Same as (c) but for correlations of  $L_s$  with snowmelt and ground temperature. The asterisks indicate that the correlations are statistically significant ( $p < 0.05$ ). All datasets used for correlations were detrended.

YRB summer precipitation; however, after the early 2000s, the positive correlation diminished dramatically and becomes non-significant. These results were robust when using different lengths for the sliding window (13, 15, and 17 years) (Supplementary Fig. 2). Since this study focused on the weakness observed in the TPWSC–EASP relationship in the early 2000s, we selected the periods 1993–2003 and 2004–2019 for further investigation, the division between these periods is based on the year when the 15-year sliding correlation drops below the 95% confidence level. The weakness in the TPWSC–EASP relationship was also clearly seen from the correlation patterns, where TPWSC displays significantly positive correlations with summer precipitation over the YRB and Northeast China, and negative correlations over South China, South Japan, and North China during the period 1993–2003 (Fig. 1c), which is consistent with the typical pattern of the TPWSC–EASP relationship<sup>10,32,33</sup>. However, correlations lost significance thereafter (Fig. 1d). This phenomenon was further reflected in the difference pattern of EASP, where the regression of EASP by TPWSC decreased over the YRB and increased over South China and North China during 2004–2019, in comparison to the period 1993–2003 (Fig. 1f).

#### Linkage between changes in TP snow cover and vegetation cover increment

Winter snow cover anomalies have significant impacts on subsequent climate due to the persistence of snow cover anomalies. Therefore, changes in snow cover and its persistence can influence the climatic effect of snow cover. Here, we examined the changes in TP snow cover during two periods 1993–2003 and 2004–2019. Notably, there were dramatic changes in TP winter

and spring snow cover after the early 2000s. Compared to the period 1993–2003, the winter snow depth and snow cover fraction over the central-eastern TP decreased during the 2004–2019 period; additionally, the time of snowmelt onset advanced to January, and the snowmelt amount in spring during the 2004–2019 period was noticeably smaller than that during the 1993–2003 period, and the memory of soil moisture related to snowmelt in spring shortened (Supplementary Fig. 3).

Snow cover distribution and snowmelt are closely related to the land surface condition. Most regions of the central-eastern TP are covered by alpine grass, and with the rise in temperature, TP has experienced an evident greening trend in past decades<sup>31</sup>. Consequently, the withered grass stems, which persist from the greening grass during the growing season, have also significantly increased (Fig. 2a). Moreover, the withered grass stems during the non-growing season (December to April) exhibit prominently interannual and interdecadal variations. After the early 2000s, the winter and spring withered grass stem area index ( $L_s$ ; see in Methods) showed a significant increase (Fig. 2b), coinciding with the period when snow cover declined and the TPWSC–EASP relationship shifts. Thus, we hypothesize that the weakening TPWSC–EASP relationship may be a result of the increment in the cover of non-growing season vegetation–withered grass stems which influences the snow cover.

To test this hypothesis, we first investigated the linkage between withered grass stems and snow cover. It is found that the withered grass stem area index ( $L_s$ ) has a significantly negative correlation with winter and spring snow depth over the central-eastern TP, so does the winter snow cover fraction (Fig. 2c); and  $L_s$  show a positive correlation with winter ground temperature and snowmelt (Fig. 2d), these correlations are also evident from the spatial pattern,

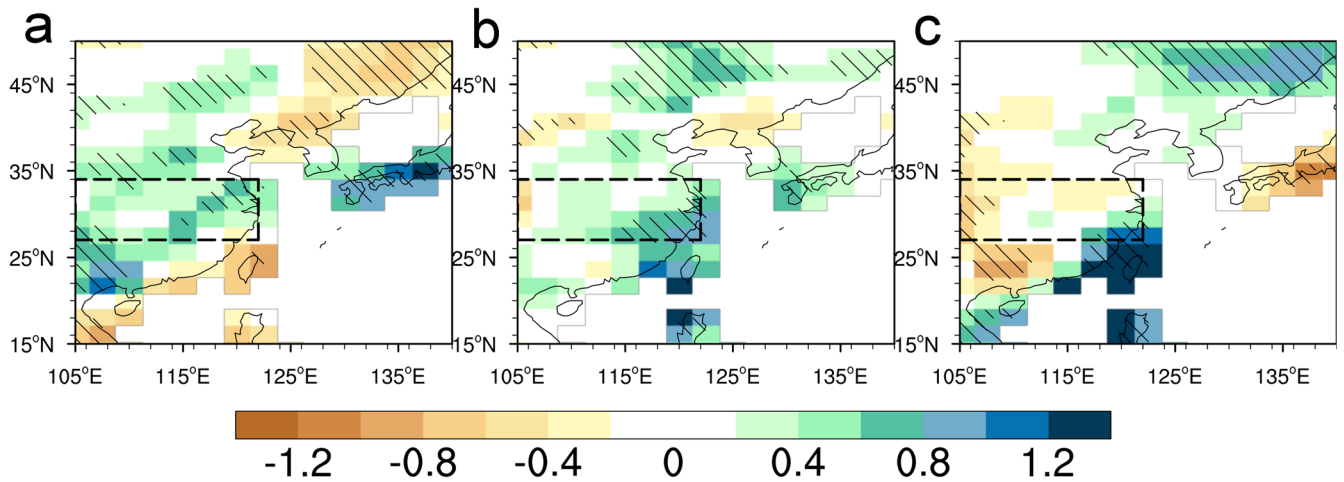


**Fig. 3 Simulated anomalies of EASP with heavier TPWSC and larger withered grass stem area.** **a** Differences of EASP ( $\text{mm day}^{-1}$ ) between experiments SNOW and CTL (SNOW minus CTL, representing impacts of heavier TPWSC), hatching shading represent the values significant at the  $p < 0.1$  confidence levels based on Student's  $t$  test. **b, c** Same as a but for differences between SNOW\_WGS and CTL (SNOW\_WGS minus CTL, representing impacts of heavier TPWSC under the condition of larger withered grass stem areas), differences between SNOW\_WGS and SNOW (SNOW\_WGS minus SNOW, representing impacts of larger withered grass stem area on climatic effects of heavier TPWSC).

significant correlations appear over regions with large snow cover interannual variability (Supplementary Fig. 4). This suggests that withered grass stem, which cannot be fully buried by shallow snow over TP, increase the ground temperature and promote the melting or sublimation of snow, thereby hindering the accumulation and preservation of snow cover in winter.

To further confirm the potential impacts of withered grass stem increment on the TPWSC–EASP relationship, we conducted three numerical experiments using the Community Earth System Model: one without (CTL) and one with (SNOW\_WGS) both heavier winter snow cover and larger withered grass stem area over central-eastern TP, one only with heavier winter snow cover (SNOW) (see Methods for details). The differences in EASP between the SNOW and CTL experiments show that when TPWSC is heavier, summer precipitation increases in the YRB and decreases in South China (Fig. 3a), this result generally reproduces the statistical TPWSC–EASP relationship observed during the period 1993–2003 (Fig. 1c). The differences in EASP between the SNOW\_WGS and CTL experiments show that summer precipitation increases in both YRB and South China (Fig. 3b). Additionally, differences in EASP between the SNOW\_WGS and SNOW experiments allow us to explore impacts of withered grass stem increment on the climatic effects of heavier TPWSC, this comparison shows that summer precipitation decreases in YRB and increases in South China (Fig. 3c). Such an opposite pattern suggests that when TPWSC is heavier under the condition of a larger withered grass stem area, the dipole pattern of summer precipitation anomalies in YRB and South China will be weakened, which is consistent with the statistical result (Fig. 1f).

### Possible mechanism behind the weakening TPWSC–EASP relationship

Statistical analyses have revealed a connection between the increment of withered grass stems and the weakening TPWSC–EASP relationship, which was confirmed through numerical experiments. Next, we used model simulations to investigate the underlying mechanism.

The model simulations show that, with heavier TPWSC, an increase in snow cover fraction and snow depth leads to cold anomalies of ground temperature through its albedo effect (Fig. 4a, b, d). This facilitates the preservation of snowpack from winter to spring, resulting in higher snowmelt amounts in April and May (Fig. 4c). However, when heavier TPWSC is accompanied by a larger

withered grass stem area, the ground albedo decreases and surface net radiation significantly increases (Supplementary Fig. 7), causing a weakness in the ground temperature anomalies induced by heavier snow cover during winter (Fig. 4d). Consequently, the anomalies of snow cover induced by both heavier TPWSC and larger WGS are smaller and disappear earlier compared to those induced by TPWSC alone (Fig. 4a, b). In other words, the weakened anomalies of ground temperature caused by the presence of withered grass stems lead to a shortened persistence of snow cover anomalies from winter to spring, primarily due to the loss of winter snow through the melting or sublimation, this is supported by the increase in 2-meter air specific humidity in December and January in experiment SNOW\_WGS (Supplementary Fig. 8).

Along with the changes in winter and spring snow cover, the resulting anomalies of surface diabatic heating over the TP exhibit distinct characteristics. The model simulations show that, with heavier TPWSC, the net longwave radiation (NLR), surface sensible heat (SH), and surface latent heat (LH) generally display negative anomalies, gradually decreasing from winter to spring, and persisting until spring (Fig. 4f, g, h). Moreover, these anomalies can even extend into summer (Supplementary Fig. 9). However, when both heavier TPWSC and larger withered grass stems are present, the NLR, SH, and LH anomalies become smaller than those induced by heavier TPWSC alone, and they tend to disappear or even reverse in the summer (Supplementary Fig. 9). These results suggest that the increment in withered grass stem alters the pattern of surface diabatic heating induced by heavier snow cover.

The diabatic heating anomalies further influence the TP thermal forcing to the atmospheric circulation in EA<sup>13,34–36</sup>. As shown in Fig. 5, the weakened TP surface diabatic heating in summer results in cold air temperature anomalies around the TP (Fig. 5a). Correspondingly, geopotential height at mid-troposphere (500 hPa) shows negative anomalies around TP, and an anomalous cyclone appears there. These anomalies propagate downstream through the excitation of a Rossby wave train<sup>33</sup>, leading to an anomalous cyclone and negative geopotential height over the region from North China to Japan (Fig. 5c). The presence of an anomalous anticyclone over the Philippines reinforces the southwesterly winds at the low-level, facilitating water vapor transport toward the YRB and resulting in increased convergence of water vapor over there, thus leading to excessive summer precipitation in the YRB (Fig. 5e). However, when heavier TPWSC occurs under the condition of a larger withered grass stem area, the disappeared or even inverted anomalies of surface



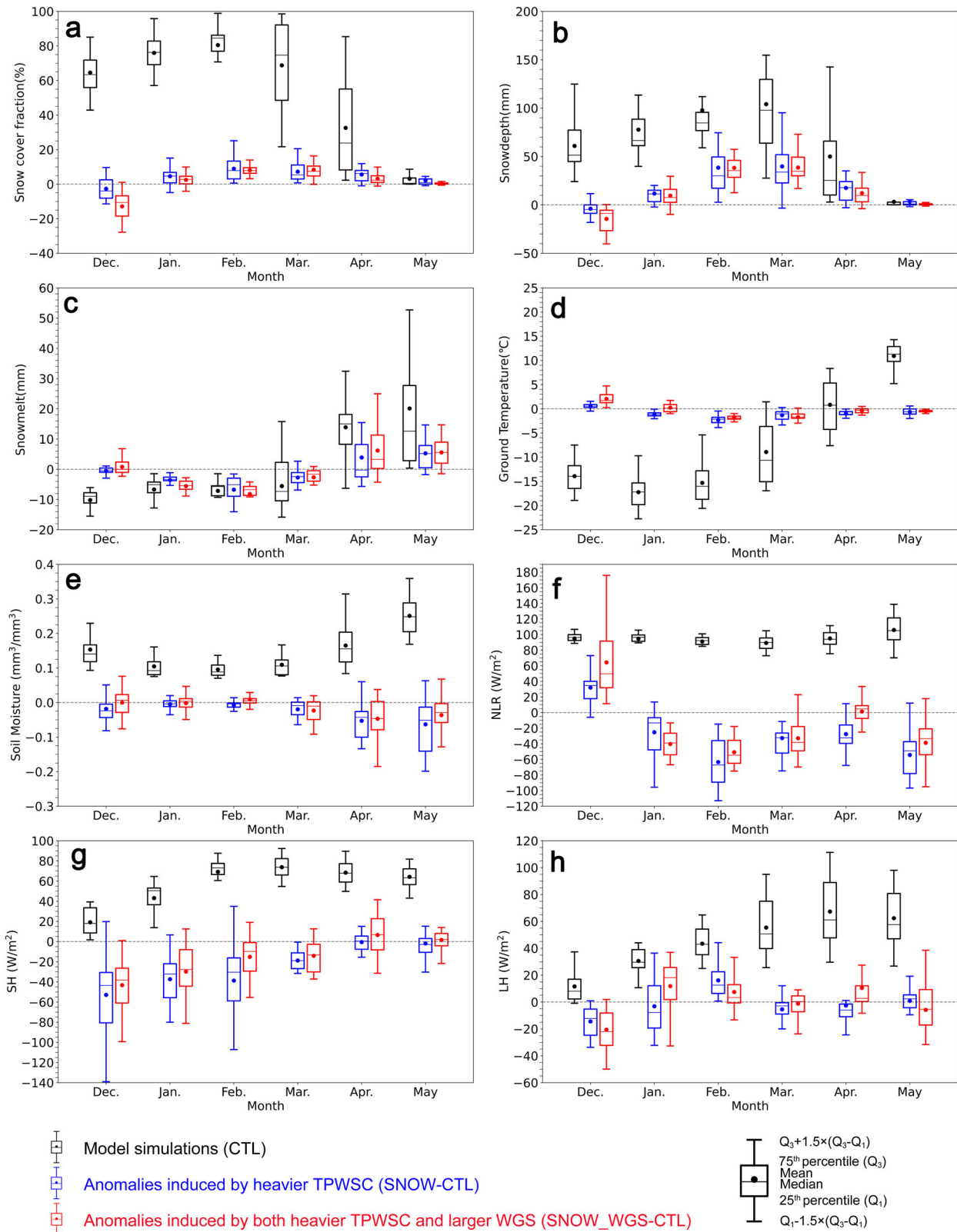


**Fig. 4** Simulated impacts of larger withered grass stem (WGS) area on snow cover and surface energy budget. **a** Box plots of simulated snow cover fraction (%) from December to May and its anomalies induced by heavier TPWSC and larger WGS. **b–h** are same as **(a)** but for snow depth (mm), snowmelt (mm), ground temperature (°C), soil moisture (liquid water;  $\text{mm}^3 \text{mm}^{-3}$ ) at depth 0–1.38 m, surface net longwave radiation (NLR;  $\text{W m}^{-2}$ ), surface sensible heat (SH;  $\text{W m}^{-2}$ ) and surface latent heat (LH;  $\text{W m}^{-2}$ ), respectively. Anomalies of soil moisture, NLR, SH and LH are amplified by 10. The statistics in the box plots from the upper to lower bound represent the value of  $Q_3 + 1.5 \times (Q_3 - Q_1)$ , third quartile ( $Q_3$ ), mean (dot), median (horizontal solid line), first quartile ( $Q_1$ ), and  $Q_1 - 1.5 \times (Q_3 - Q_1)$  successively. The value of  $Q_3 - Q_1$  denotes the interquartile range.

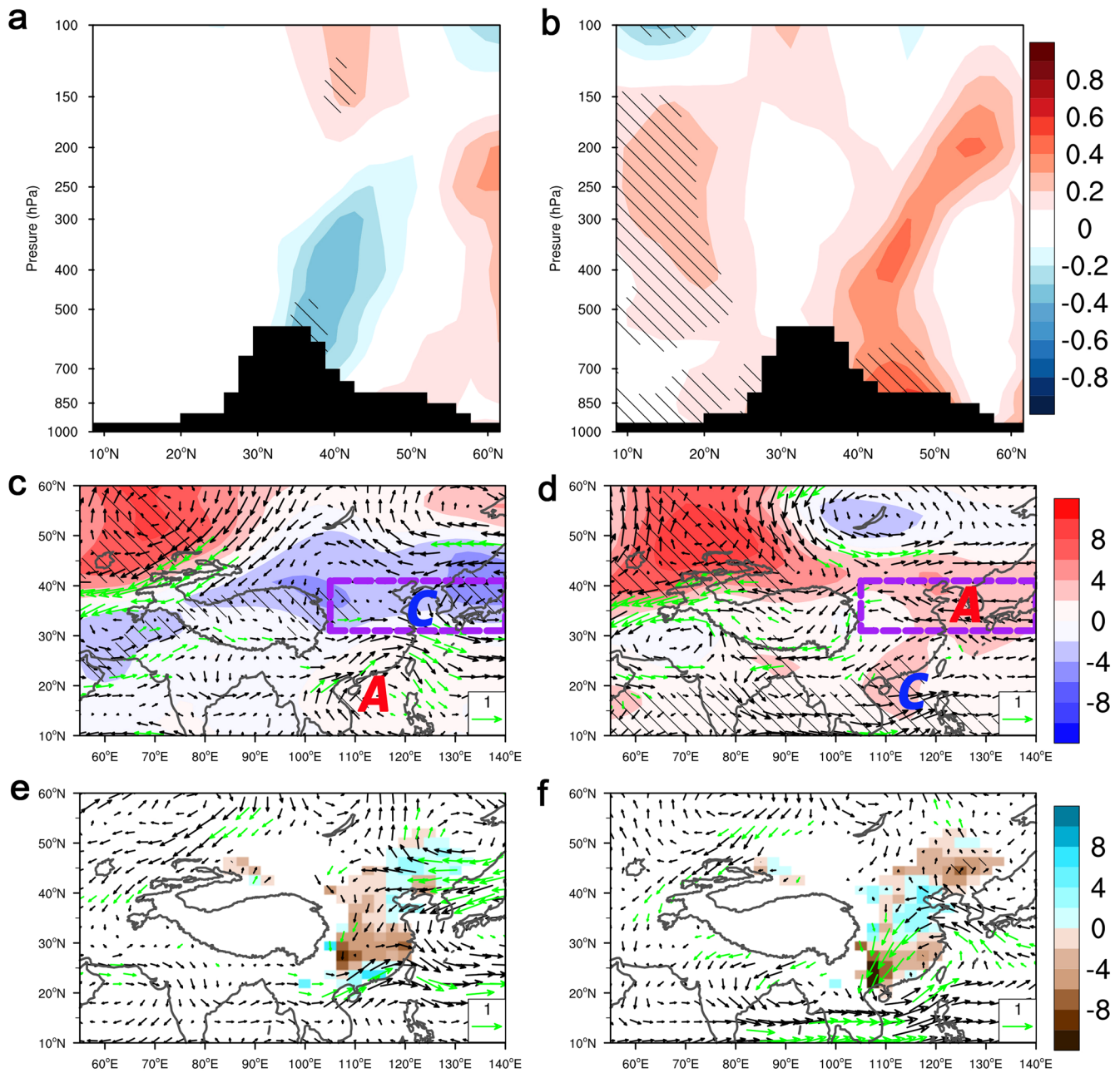


**Fig. 5** Impacts of TPWSC anomalies on atmospheric circulation around the TP and over EA in summer (June–July–August). Latitude–height cross-sections (80°–100°E average) of anomalies of air temperature (°C) from experiments (a) SNOW and (b) SNOW\_WGS, respectively. Simulated anomalies of geopotential height (color shading; gpm) and horizontal wind (vectors;  $\text{m s}^{-1}$ ) at 500 hPa from experiments c) SNOW and d) SNOW\_WGS, respectively. In the panel, alphabet “A” and “C” represent anomalous anticyclones and cyclones, respectively. e, f Same as c, d but for water vapor flux divergence (color shading;  $10^{-9} \text{ g s}^{-1} \text{ cm}^{-2} \text{ hPa}^{-1}$ ) and horizontal wind (vectors;  $\text{m s}^{-1}$ ) at 850 hPa. Slashed shading, and green vectors represent anomalies values significant at the  $p < 0.1$  confidence level based on Student’s  $t$  test.

diabatic heating in the summer lead to warm air temperature anomalies around the TP in the middle-upper troposphere, especially on the north side of the TP (Fig. 5b). Consequently, positive anomalies of geopotential height and an anomalous anticyclone appear over the north side of the TP (Fig. 5d), leading to an anomalous anticyclone over the region from North China to Japan, and the accompanying anomalous cyclone over the South China Sea weakens the southwesterly winds at the low-level, resulting in decreased water vapor convergence over the YRB (Fig. 5f), this makes the positive impact of TPWSC anomalies on summer precipitation over the YRB non-significant. The model simulations are consistent

with the anomaly patterns of geopotential height and horizontal wind regressed against the TPWSC (Supplementary Fig. 10).

## DISCUSSIONS

In this study, we elucidated the significant changes in the TPWSC–EASP relationship on an interdecadal scale over the past 40 years (1980–2019). The weakening TPWSC–EASP relationship observed after the early 2000s was found to be closely related to the increment in the cover of non-growing season vegetation–withered grass stem. The presence of withered grass stems impact ground temperature by reducing the ground albedo

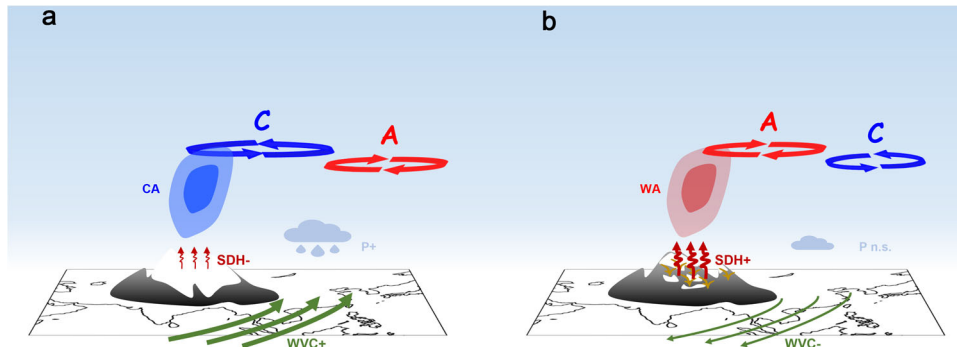


**Fig. 6 Schematic diagram of impacts of withered grass stem area increment on TPWSC–EASP relationship.** **a** When TPWSC is heavier, TP surface diabatic heating (SDH) in summer is weakened, leading to cold anomalies (CA) of air temperature around TP, consequently, an anomalous cyclone and an anomalous anticyclone appear over North China and the Philippines, respectively, resulting in the enhanced water vapor convergence (WVC) and excessive summer precipitation (P) over YRB. **b** When TPWSC is heavier with presence of larger withered grass stem area, snow cover anomalies cannot persist throughout the entire spring, summer SDH is enhanced, leading to warm anomalies (WA) of air temperature around TP, consequently, an anomalous anticyclone and an anomalous cyclone appear over North China and the Philippines, respectively, resulting in the weakened WVC and non-significant (n.s.) anomalies of summer precipitation over YRB. Alphabet “A” and “C” represent anomalous anticyclone and cyclones, respectively. “+” and “–” in the panel represent enhanced and weakened anomalies.

and increasing the radiation absorbed by the land surface, which accelerates the loss of snow cover, leading to a shortened persistence of snow cover anomalies from winter to spring. Consequently, the surface diabatic heating anomalies in summer, which were connected to TPWSC, were reversed. As a result, atmospheric circulation in EA shows a different anomalous pattern, and the impacts of TPWSC anomalies on EASP were altered (Fig. 6). Results of this study highlight that the presence of withered grass stems that are not buried by snow can significantly alter the surface energy budget, thereby influencing the snow cover dynamics<sup>29</sup>, especially for vegetation that has experienced growth in recent decades<sup>31</sup>. Thus, the influence of vegetation cover increment on the lagged effects of snow cannot be overlooked. The findings of this study have the potential to be extended to better understand snow–vegetation feedback in the high latitudes of the Northern Hemisphere.

Studies have shown that sea surface temperature anomalies over middle-east equator Pacific Ocean<sup>37</sup>, tropical Indian Ocean<sup>38</sup>, and North Atlantic Ocean<sup>39</sup> have impacts on East Asian summer climate on an interdecadal scale. Here, we examined the relationship between TPWSC and EASP after removing the influences of various factors such as ENSO (El Niño–Southern Oscillation), IOD (Indian Ocean Dipole), NAO (North Atlantic Oscillation), and other interdecadal and multidecadal oscillations, such as AMO (Atlantic Multidecadal Oscillation) and PDO (Pacific Decadal Oscillation). We found that the TPWSC–EASP relationship still exhibits robust interdecadal changes, it implies that the TPWSC–EASP relationship is independent and its interdecadal changes appear to be related to the snow process itself.

It also should be noted that a numerical model was employed to explore the potential impacts of VCI on the TPWSC–EASP relationship, simulation results generally validate the statistical diagnoses; however, due to the incomplete parameterizations related to snow–vegetation processes (e.g., constant assumption of grass canopy height) and possible noise mixed in diagnostic results, there may be some discrepancies between the model simulations and the statistical diagnoses. Nevertheless, the model simulations partially demonstrate the impacts of VCI on winter and spring snow cover, surface energy budget, and their role in contributing to changes in the TPWSC–EASP relationship. Hence, an improved model that incorporates a more accurate representation of the interactions between snow and vegetation is necessary to further deepen our understanding of the feedback between vegetation cover changes and snow dynamics. In addition, the

proportion of snowmelt contributing to soil moisture (snow hydrological effects) is influenced by the soil infiltration capacity, which is affected by the soil freeze–thaw process<sup>40</sup>. With permafrost degradation, the earlier onset of soil thaw and deepening of the active layer thickness could enhance the infiltration of snowmelt water into the soil and contribute to soil moisture in spring<sup>41</sup>, which has considerable impacts on the land–atmosphere interaction<sup>42</sup>. Investigating the role of permafrost degradation in the lagged effects of snow needs in future studies.

## METHODS

### Data

**Remote sensing snow cover and depth.** The weekly Northern Hemisphere snow cover extent data<sup>43</sup> of version 4 from the National Snow and Ice Data Center (NSIDC) for 1979–2019 with Equal-Area Scalable Earth (EASE) Grid 2.0 projection at a 25-km spatial resolution was used. The weekly EASE-Grid SCE data were converted to monthly mean snow cover fraction data on regular  $1^\circ \times 1^\circ$  grids. The daily snow depth dataset for 1979–2019 derived from SMMR, SSM/I, and AMSR-E passive microwave remote sensing data with a horizontal resolution of  $0.25^\circ \times 0.25^\circ$  was used<sup>44</sup>. The monthly snow depth data on  $1^\circ \times 1^\circ$  grids were averaged from the daily dataset.

**precipitation data.** Monthly precipitation data at a  $1^\circ \times 1^\circ$  spatial resolution during 1980–2019 were obtained from the Global Precipitation Climatology Centre (GPCC)<sup>45</sup>.

**Conversion of stem area index ( $L_s$ ) from leaf area index (LAI).** Adopting the method from Zeng et al.<sup>46</sup>,  $L_s$  can be calculated as:

$$L_s^n = \max\left\{ \left[ aL_s^{n-1} + \max\left( L_{gv}^{n-1} - L_{gv}^n, 0 \right) \right], L_{s,\min} \right\} \quad (1)$$

where  $L_{gv} = LAI/\sigma_v$  and  $\sigma_v$  is the fractional vegetation cover,  $n$  denotes the  $n$ th month,  $L_{s,\min}$  denotes the prescribed minimum value of  $L_s$ , and  $a$  denotes the monthly residual rate of stem and dead leaves. The satellite-derived LAI data from 1982–2018 was obtained from the Global Land Surface Satellite (GLASS) product<sup>47</sup>, which is generated using general regression neural networks (GRNNs) that are trained using the integrated satellite LAI time-series and the Moderate Resolution Imaging Spectroradiometer (MODIS) surface reflectance data or the Advanced Very-High-Resolution Radiometer (AVHRR) surface reflectance data, with a



temporal resolution of 8 days and a spatial resolution of  $0.05^\circ$ . We resample the stem area index data into  $1^\circ \times 1^\circ$  spatial resolution to match the resolution of other datasets. In this study, areas with grass coverage exceeding 50% were classified as grassland,  $L_s$  in grassland represent the withered grass stem area.

**Climatic variables.** The monthly ground temperature, geopotential height, and meridional and zonal winds were obtained from the fifth-generation ECMWF (European Centre for Medium-Range Weather Forecasts) reanalysis (ERA5) for the global climate and weather for the period from 1980 to 2019 at a spatial resolution of  $1^\circ \times 1^\circ$ . Multivariate El Niño–Southern Oscillation (ENSO) Index (MEI)<sup>48</sup> data for the period from 1979 to 2019 were obtained from the NOAA Earth System Research Laboratory. The IOD (Indian Ocean Dipole), NAO (North Atlantic Oscillation), AMO (Atlantic Multidecadal Oscillation), PDO (Pacific Decadal Oscillation), and AO (Arctic Oscillation) data were also obtained from NOAA Climate Prediction Center (CPC).

### Tibetan Plateau winter snow cover (TPWSC) index and East Asia summer precipitation (EASP)

To extract the anomalies of TP winter snow cover (TPWSC), the empirical orthogonal function (EOF) was employed for snow cover fraction (time series are detrended), we chose leading EOF mode (EOF1) as the pattern of interannual spatiotemporal variability of TP winter snow cover fraction. The standardization of the December, January, and February (DJF) snow cover fraction averaged over the central-eastern TP ( $31^\circ$ – $36^\circ$ N,  $85^\circ$ – $100^\circ$ E) where TPWSC has large interannual variability was defined as the TPWSC index. Interannual variability in TPWSC is highly consistent with those in PC1 (Supplementary Fig. 1), indicating that this index can provide a feasible representation of the spatiotemporal variability in winter snow cover over the TP during the 1980–2019 period.

The EASP refers to the summer land precipitation over East Asia ( $15^\circ$ – $50^\circ$ N,  $105^\circ$ – $140^\circ$ E). For statistical analyses, summer precipitation averaged over Yangtze River Basin ( $27^\circ$ – $34^\circ$ N,  $105^\circ$ – $122^\circ$ E) is calculated as an index that represents the temporal variations of EASP.

### Definition and quantization of snowmelt

Snowmelt is difficult to measure directly but can be reasonably derived from snow depletion<sup>22</sup>. Snow depletion is calculated as the difference between the snow water equivalent ( $W$ ;  $\text{kg m}^{-2}$ ) between the current month ( $M$ ) and the preceding month ( $M - 1$ ):

$$\Delta W = W_{M-1} - W_M = d_{M-1} \cdot \rho_{M-1} - d_M \cdot \rho_M = \Delta d \cdot \rho_{M-1} - d_M \cdot (\rho_M - \rho_{M-1}) \quad (2)$$

Where  $\Delta W$  is not only determined by snow depth changes ( $\Delta d$ ; m) but also related to snow density changes ( $\rho_M - \rho_{M-1}$ ;  $\text{kg m}^{-3}$ ) caused by snow metamorphism, load or overburden. However, due to the unavailable long-time series observations and large biases of the grid-point dataset of snow water equivalent over the TP<sup>49</sup>, snow depth changes ( $\Delta d$ ) are used as a proxy for snowmelt in this study. Although the snow density in spring is generally larger than that in winter<sup>50</sup>, spring snowmelt based on  $\Delta d$  might be overestimated. Nevertheless, a directly proportional relationship between  $\Delta W$  and  $\Delta d$  means that the interannual variability in snowmelt can be represented by snow depth changes. The monthly snowmelt is defined as the difference between snow depth ( $d$ ) in the current month ( $M$ ) and the preceding month ( $M - 1$ ):

$$\Delta d = d_{M-1} - d_M \quad (3)$$

### Extracting the independent relationship between TPWSC and EASP

To focus on the impacts of interannual and decadal variations in snow cover anomalies over the TP, all datasets used for correlation

and regression analysis were detrended. To exclude the impacts of ocean and other interdecadal and multidecadal oscillations, the snow cover fraction, precipitation, stem area index ( $L_s$ ), ground temperature, and atmospheric variables (geopotential height, horizontal wind) regressed against the ENSO (El Niño–Southern Oscillation), IOD (Indian Ocean Dipole) and NAO (North Atlantic Oscillation), AMO (Atlantic Multidecadal Oscillation) and PDO (Pacific Decadal Oscillation) were subtracted one by one.

### Numerical experiments

To validate the impact of VCI on the TPWSC–EASP relationship, the Community Earth System Model version 2.2.0 (CESM2.2.0) developed by the U.S. National Center for Atmospheric Research (NCAR) was utilized, CESM has been widely used in simulation studies over TP and has the ability to simulate the climate and large-scale atmospheric circulation over EA<sup>13,24,51</sup>. The land component of CESM2.2.0, the Community Land Model version 5.0 (CLM5.0), has been improved in snow parameterizations<sup>52</sup>, and it can well simulate the distribution of winter and spring snow cover over TP (Supplementary Fig. 5). Three groups of numerical experiments were conducted. In the control experiment (CTL), both the grass stem area index and snow cover remained unchanged. In the first sensitive experiment (SNOW), we imposed heavier winter snow cover over TP by increasing the winter (December–January–February) snowfall rate by 50% over central-eastern TP ( $31^\circ$ – $36^\circ$ N,  $85^\circ$ – $100^\circ$ E) where TPWSC has large interannual variability. In the second sensitive experiment (SNOW\_WGS), we not only increased the winter snowfall rate by 50% but also simultaneously raised the grass stem area index ( $L_s$ ) over central-eastern TP from December to May by 50% over central-eastern TP (Supplementary Fig. 6). In all experiments, CESM was run with coupled atmosphere and land, the sea surface temperature and sea ice conditions were set to climatological distributions (component set F2000climo). The simulations were integrated for 25 years, with the first 5 years for spin-up, the remaining 20 years of simulations were regarded as the 20 ensembles for each experiment. The differences between SNOW and CTL represent anomalies induced by heavier TPWSC alone, differences between SNOW\_WGS and CTL represent anomalies induced by both heavier TPWSC and a larger withered grass stem area, while differences between SNOW\_WGS and SNOW represent anomalies induced by a larger withered grass stem area.

### DATA AVAILABILITY

The weekly Northern Hemisphere snow cover extent data of NSIDC is available from <https://nsidc.org/data/nsidc-0046>. The daily snow depth dataset can be downloaded from <http://poles.tpdc.ac.cn/en/data/df40346a-0202-4ed2-bb07-b65dfcda9368/>. The Monthly precipitation data of GPCC is got from <https://www.psl.noaa.gov/data/gridded/data.gpcc.html>. The LAI data of AVHRR is available from <http://www.glass.umd.edu/LAI/AVHRR/>. The ERA5 reanalysis data used in this study are available from the Copernicus Climate Data Store at <https://cds.climate.copernicus.eu/>. The Multivariate El Niño–Southern Oscillation (ENSO) Index (MEI) data is obtained from <https://psl.noaa.gov/enso/mei/>. The IOD index data can be download from [https://psl.noaa.gov/gcos\\_wgsp/Timeseries/DMI/](https://psl.noaa.gov/gcos_wgsp/Timeseries/DMI/). The NAO index can be obtained from <https://www.cpc.ncep.noaa.gov/products/precip/CWlink/pna/norm.nao.monthly.b5001.current.ascii.table>. The PDO index can be obtained from <https://www.ncei.noaa.gov/access/monitoring/pdo/>. The AMO index can be obtained from <https://climatedataguide.ucar.edu/climate-data/atlantic-multi-decadal-oscillation-amo>. The AO index can be obtained from [https://www.cpc.ncep.noaa.gov/products/precip/CWlink/daily\\_ao\\_index/ao.shtml](https://www.cpc.ncep.noaa.gov/products/precip/CWlink/daily_ao_index/ao.shtml).

### CODE AVAILABILITY

The source codes of CESM2.2.0 can be obtained from <https://github.com/ESCOMP/CESM/tree/release-cesm2.2.0>. All data processing codes for the analysis of this study are available from the corresponding author upon reasonable request.



Received: 30 March 2023; Accepted: 30 August 2023;  
Published online: 12 September 2023

## REFERENCES

- Barnett, T., Dumenil, L., Schlese, U., Roeckner, E. & Latif, M. The effect of Eurasian snow cover on regional and global climate variations. *J. Atmos. Sci.* **46**, 661–685 (1989).
- Cohen, J. & Rind, D. The effect of snow cover on the climate. *J. Clim.* **4**, 689–706 (1991).
- Xu, L. & Dirmeyer, P. Snow-atmosphere coupling strength in a global atmospheric model. *Geophys. Res. Lett.* **38**, L13401 (2011).
- Orsolini, Y. J. et al. Impact of snow initialization on sub-seasonal forecasts. *Clim. Dyn.* **41**, 1969–1982 (2013).
- Tang, S. et al. Regional and tele-connected impacts of the Tibetan Plateau surface darkening. *Nat. Commun.* **14**, 32 (2023).
- Ghatak, D., Sinsky, E. & Miller, J. Role of snow-albedo feedback in higher elevation warming over the Himalayas, Tibetan Plateau and Central Asia. *Environ. Res. Lett.* **9**, 114008 (2014).
- Guo, H. et al. Spring snow-albedo feedback analysis over the third pole: results from satellite observation and CMIP5 model simulations. *J. Geophys. Res. -Atmos.* **123**, 750–763 (2018).
- Blanford, H. F. On the connexion of the Himalaya snowfall with dry winds and seasons of drought in India. *Proc. R. Soc. Lond.* **37**, 3–22 (1884).
- Wei, Z., Luo, S. & Dong, W. Snow cover data on Qinghai-Xizang Plateau and its correlation with summer rainfall in China. *Quart. J. Appl. Meteor.* **9**, 39–46 (1998).
- Chen, L. T. & Wu, R. G. Interannual and decadal variations of snow cover over Qinghai-Xizang Plateau and their relationships to summer monsoon rainfall in China. *Adv. Atmos. Sci.* **17**, 18–30 (2000).
- Wu, R. & Kirtman, B. P. Observed relationship of spring and summer East Asian rainfall with winter and spring Eurasian snow. *J. Clim.* **20**, 1285–1304 (2007).
- Chen, H., Qi, D. & Xu, B. Influence of snow melt anomaly over the mid-high latitudes of the Eurasian continent on summer low temperatures in northeastern China. *Chin. J. Atmos. Sci.* **37**, 1337–1347 (2013).
- Wang, C., Yang, K., Li, Y., Wu, D. & Bo, Y. Impacts of spatiotemporal anomalies of Tibetan Plateau snow cover on summer precipitation in Eastern China. *J. Clim.* **30**, 885–903 (2017).
- Li, W. et al. Influence of Tibetan Plateau snow cover on East Asian atmospheric circulation at medium-range time scales. *Nat. Commun.* **9**, 4243 (2018).
- Chen, L. Test and application of the relationship between anomalous snow cover in winter-spring over Qinghai-Xizang Plateau and the first summer precipitation in South China. *Quart. J. Appl. Meteor.* **9**, 1–8 (1998).
- Chen, L. The role of the anomalous snow cover over the Qinghai-Xizang Plateau and ENSO in the great floods of 1998 in the Changjiang River valley. *Chin. J. Atmos. Sci.* **25**, 184–192 (2001).
- Li, P. J. Response of Tibetan snow cover to global warming (in Chinese). *Acta Geogr. Sin.* **51**, 260–265 (1996).
- Zhang, Y. S., Li, T. & Wang, B. Decadal change of the spring snow depth over the Tibetan Plateau: the associated circulation and influence on the East Asian summer monsoon. *J. Clim.* **17**, 2780–2793 (2004).
- Shen, S. S. P. et al. Characteristics of the Tibetan Plateau snow cover variations based on daily data during 1997–2011. *Theor. Appl. Climatol.* **120**, 445–453 (2015).
- Richardson, A. D. et al. Climate change, phenology, and phenological control of vegetation feedbacks to the climate system. *Agric. Meteorol.* **169**, 156–173 (2013).
- Musselman, K. N., Clark, M. P., Liu, C., Ikeda, K. & Rasmussen, R. Slower snowmelt in a warmer world. *Nat. Clim. Chang.* **7**, 214–219 (2017).
- Wu, X., Che, T., Li, X., Wang, N. & Yang, X. Slower snowmelt in spring along with climate warming across the Northern Hemisphere. *Geophys. Res. Lett.* **45**, 12331–12339 (2018).
- Zhang, T. et al. The weakening relationship between Eurasian spring snow cover and Indian summer monsoon rainfall. *Sci. Adv.* **5**, eaau8932 (2019).
- Wang, Z. et al. Decreasing influence of summer snow cover over the Western Tibetan Plateau on East Asian precipitation under global warming. *Front. Earth Sci.* **9**, 787971 (2021).
- Zhang, C., Guo, Y. & Wen, Z. Interdecadal change in the effect of Tibetan Plateau snow cover on spring precipitation over Eastern China around the early 1990s. *Clim. Dyn.* **58**, 2807–2824 (2022).
- Clark, M. P. et al. Representing spatial variability of snow water equivalent in hydrologic and land-surface models: a review. *Water Resour. Res.* **47**, W07539 (2011).
- Qian, Y., Flanner, M. G., Leung, L. R. & Wang, W. Sensitivity studies on the impacts of Tibetan Plateau snowpack pollution on the Asian hydrological cycle and monsoon climate. *Atmos. Chem. Phys.* **11**, 1929–1948 (2011).
- Gusev, Y. M. & Nasonova, O. N. The simulation of heat and water exchange in the boreal spruce forest by the land-surface model SWAP. *J. Hydrol.* **280**, 162–191 (2003).
- Wang, A. H. & Zeng, X. Improving the treatment of the vertical snow burial fraction over short vegetation in the NCAR CLM3. *Adv. Atmos. Sci.* **26**, 877–886 (2009).
- Jiang, Y. et al. Assessment of uncertainty sources in snow cover simulation in the Tibetan Plateau. *J. Geophys. Res. -Atmos.* **125**, e2020JD032674 (2020).
- Shen, M. et al. Evaporative cooling over the Tibetan Plateau induced by vegetation growth. *Proc. Natl Acad. Sci. USA* **112**, 9299–9304 (2015).
- Wu, T. W. & Qian, Z. A. The relation between the Tibetan winter snow and the Asian summer monsoon and rainfall: an observational investigation. *J. Clim.* **16**, 2038–2051 (2003).
- Wang, B., Bao, Q., Hoskins, B., Wu, G. & Liu, Y. Tibetan plateau warming and precipitation changes in East Asia. *Geophys. Res. Lett.* **35**, L14702 (2008).
- Duan, A. M. & Wu, G. X. Role of the Tibetan Plateau thermal forcing in the summer climate patterns over subtropical Asia. *Clim. Dyn.* **24**, 793–807 (2005).
- Duan, A., Wang, M., Lei, Y. & Cui, Y. Trends in summer rainfall over China associated with the Tibetan Plateau sensible heat source during 1980–2008. *J. Clim.* **26**, 261–275 (2013).
- Wu, G. et al. Thermal controls on the Asian Summer monsoon. *Sci. Rep.* **2**, 404 (2012).
- Yim, S. Y., Jhun, J. G. & Yeh, S. W. Decadal change in the relationship between East Asian–western North Pacific summer monsoons and ENSO in the mid-1990s. *Geophys. Res. Lett.* **35**, L20711 (2008).
- Sun, B., Li, H. & Zhou, B. Interdecadal variation of Indian Ocean basin mode and the impact on Asian summer climate. *Geophys. Res. Lett.* **46**, 12388–12397 (2019).
- Sun, J., Wang, H. & Yuan, W. Decadal variations of the relationship between the summer North Atlantic Oscillation and middle East Asian air temperature. *J. Geophys. Res.* **113**, D15107 (2008).
- Swenson, S. C., Lawrence, D. M. & Lee, H. Improved simulation of the terrestrial hydrological cycle in permafrost regions by the Community Land Model. *J. Adv. Model. Earth Syst.* **4**, M08002 (2012).
- Yang, K. & Wang, C. Frozen soil advances the effect of spring snow cover anomalies on subsequent precipitation over Tibetan Plateau. *J. Hydrometeorol.* **24**, 335–350 (2023).
- Yang, K. & Wang, C. East–west reverse coupling between Spring soil moisture and summer precipitation and its possible responsibility for wet bias in GCMs over Tibetan Plateau. *J. Geophys. Res. -Atmos.* **127**, e2021JD036286 (2022).
- Brodzik, M. J. & Armstrong, R. Northern Hemisphere EASE-Grid 2.0 weekly snow cover and sea ice extent, version 4 (Boulder, CO: NASA National Snow and Ice Data Center). <https://doi.org/10.5067/P700HGJLYUQU> (2013).
- Che, T., Li, X., Jin, R., Armstrong, R. & Zhang, T. Snow depth derived from passive microwave remote-sensing data in China. *Ann. Glaciol.* **49**, 145–154 (2008).
- Schneider, U. et al. Evaluating the hydrological cycle over land using the newly-corrected precipitation climatology from the global precipitation climatology centre (GPCC). *Atmosphere* **8**, 52 (2017).
- Zeng, X., Shaikh, M., Dai, Y., Dickinson, R. E. & Myneni, R. Coupling of the Common Land Model to the NCAR Community Climate Model. *J. Clim.* **15**, 1832–1854 (2002).
- Liang, S. et al. The Global Land Surface Satellite (GLASS) Product Suite. *Bull. Am. Meteorol. Soc.* **102**, 323–337 (2021).
- Wolter, K. & Timlin, M. S. El Niño/Southern Oscillation behaviour since 1871 as diagnosed in an extended multivariate ENSO index (MEI.ext). *Int. J. Climatol.* **31**, 1074–1087 (2011).
- Liu, Y., Fang, Y., Li, D. & Margulis, S. A. How well do global snow products characterize snow storage in High Mountain Asia? *Geophys. Res. Lett.* **49**, e2022GL100082 (2022).
- Niu, G.-Y. & Yang, Z.-L. An observation-based formulation of snow cover fraction and its evaluation over large North American river basins. *J. Geophys. Res. -Atmos.* **112**, D21101 (2007).
- Yang, K. & Wang, C. Seasonal persistence of soil moisture anomalies related to freeze-thaw over the Tibetan Plateau and prediction signal of summer precipitation in eastern China. *Clim. Dyn.* **53**, 2411–2424 (2019).
- Lawrence, D. M. et al. The Community Land Model version 5: description of new features, benchmarking, and impact of forcing uncertainty. *J. Adv. Model. Earth Syst.* **11**, 4245–4287 (2019).

## ACKNOWLEDGEMENTS

This work was supported by the National Natural Science Foundation of China (42305017, 42175064, 91837205), Natural Science Foundation of Gansu Province (22JR5RA442).

## AUTHOR CONTRIBUTIONS

K.Y. and C.W. conceptualized the study. K.Y. conducted the numerical experiments. K.Y. and Q.Q. contributed to data analysis. K.Y. interpreted the results and wrote the drafts. All contributes to review and improve the manuscript.

## COMPETING INTERESTS

The authors declare no competing interests.

## ADDITIONAL INFORMATION

**Supplementary information** The online version contains supplementary material available at <https://doi.org/10.1038/s41612-023-00467-3>.

**Correspondence** and requests for materials should be addressed to Kai Yang or Chenghai Wang.

**Reprints and permission information** is available at <http://www.nature.com/reprints>

**Publisher's note** Springer Nature remains neutral with regard to jurisdictional claims in published maps and institutional affiliations.



**Open Access** This article is licensed under a Creative Commons Attribution 4.0 International License, which permits use, sharing, adaptation, distribution and reproduction in any medium or format, as long as you give appropriate credit to the original author(s) and the source, provide a link to the Creative Commons license, and indicate if changes were made. The images or other third party material in this article are included in the article's Creative Commons license, unless indicated otherwise in a credit line to the material. If material is not included in the article's Creative Commons license and your intended use is not permitted by statutory regulation or exceeds the permitted use, you will need to obtain permission directly from the copyright holder. To view a copy of this license, visit <http://creativecommons.org/licenses/by/4.0/>.

© The Author(s) 2023